International Journal of Mechanical, Industrial and Aerospace Sciences
ISSN: 2517-9950
Vol:11, No:3, 2017

Characteristics of Ozone Generated from Dielectric Barrier Discharge Plasma Actuators

R. Osada, S. Ogata, T. Segawa

***Abstract*—**Dielectric barrier discharge plasma actuators (DBD-PAs) have been developed for active flow control devices. However, it is necessary to reduce ozone produced by DBD toward practical applications using DBD-PAs. In this study, variations of ozone concentration, flow velocity, power consumption were investigated by changing exposed electrodes of DBD-PAs. Two exposed electrode prototypes were prepared: span-type with exposed electrode width of 0.1 mm, and normal-type with width of 5 mm. It was found that span-type shows lower power consumption and higher flow velocity than that of normal-type at $V_{p\text{-}p}$ = 4.0-6.0 kV. Ozone concentration of span-type higher than normal-type at $V_{p\text{-}p}$ = 4.0-8.0 kV. In addition, it was confirmed that catalyst located in downstream from the exposed electrode can reduce ozone concentration between 18 and 42% without affecting the induced flow.

***Keywords*—**Dielectric barrier discharge plasma actuators, ozone diffusion, PIV measurement, power consumption.

I. Introduction

DBD-PAs were developed by Roth et al. in the late 1990s as simple fluid control devices without mechanical moving parts [1]. As indicated in Fig. 1, DBD-PAs have an extremely simple structure comprised of two asymmetrically arranged electrodes, and a dielectric interposed between them. If high voltage is applied at high frequency to the electrodes, a DBD occurs near the edge on one side of the exposed electrode, and near the wall surface pole an induced flow is produced in the direction from the exposed electrode to the encapsulated electrode. Fluid control using DBD-PAs has various advantages, such as: (1) Enabling induction of local body force near the wall surface, (2) Enabling electrical control with short time constant, (3) No mechanical moving parts to cause secondary flow, and (4) A simple, soft structure comprised of the layered electrodes and dielectric. The technique has achieved significant results in the fields of separation control and noise reduction control [2]-[6]. On the other hand, there are challenges for practical application, such as: (1) Power supply equipment is needed to output high voltage, (2) Low durability due to dielectric insulation damage cause by electric discharge etc., (3) Low conversion efficiency of about 0.1% from electrical energy to kinetic energy acquired by fluid, and (4) Generation of ozone (harmful to the human body) due to the occurrence of DBD. As part of efforts to improve performance of DBD-PAs, Hagiwara et al. showed that thinning exposed electrode increases induced flow velocity, and broadens the plasma generation region [7]. Thinning improves the kinetic energy conversion efficiency of DBD-PAs, but this may also lead to increase in generated ozone. Ozone has high oxidizing power, second only to fluorine, and thus industrially it is a beneficial gas used as a substitute for chlorine in tasks such as sterilization and bleaching. However, it also carries risks, such as causing insulation destruction or damage, as a result of deterioration of the dielectric in DBD-PAs. In addition, industrial safety and health standards stipulate of Japan that the ozone concentration of indoor air must be less than 0.1 ppm, and this is an unavoidable issue for practical application in fluid equipment.

In terms of research in recent years on ozone generated from DBD-PAs, Kawamoto et al. have reported that, when AC voltage with $V_{p\text{-}p}$ = 6.0 kV and frequency of f_p = 1.0 kHz was applied to DBD-PAs with an electrode length of 22 mm, high-concentration ozone of about 100 ppm was detected [8]. Nicole et al. have shown that ozone concentration increases together with voltage and frequency applied to DBD-PAs [9]. However, there have been no reports in previous research on the spatial distribution of ozone diffusion generated from DBD-PAs, or on techniques for reducing that diffusion. Therefore, the purpose of this research is to investigate based on an experimental approach the distribution of ozone generated from DBD-PAs, the effects of electrode geometry on ozone concentration, induced flow velocity and power consumption. This study also investigates techniques, using catalysts and carbon sheets to break down ozone, to efficiently reduce without affecting induced flow.

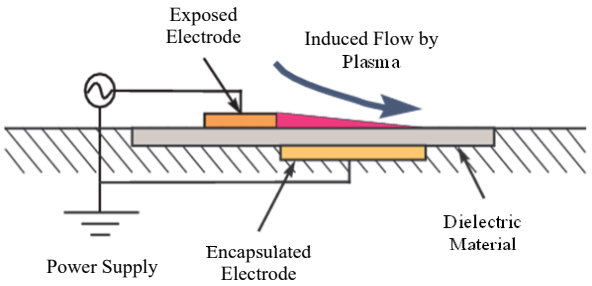

Fig. 1 Structure of DBD-PAs

R. Osada is with the Tokyo Metropolitan University, Minami Osawa 1-1, Hachioji-shi, Tokyo, Japan (phone: +81-042-677-1111 (Ext. 4195); e-mail: osada-ryo@ed.tmu.ac.jp).
S. Ogata is with the Tokyo Metropolitan University, Minami Osawa 1-1, Hachioji-shi, Tokyo, Japan (e-mail: ogata-satoshi@tmu.ac.jp).
T. Segawa is with the National Institute of Advanced Industrial Science and Technology (AIST), Namiki 1-2-1, Tsukuba-shi, Ibaraki, Japan (e-mail: t-segawa@aist.go.jp).

II. Experimental Apparatus and Method

A. Electrode Geometry of DBD-PAs

As the material of the DBD-PAs, a Teflon double-sided copper-clad laminated plate was used in which cooper foil (35 μm) was roll bonded onto both sides (front and back) of the Teflon plate which acts as the dielectric (160 μm, permittivity, $\varepsilon' \approx 2$). The copper foil surface was fabricated by aligning copper foil surfaces on both sides using a PCB process, and performing etching. In this research, the ozone concentration, power consumption and induced flow velocity were compared for different geometries of the exposed electrode, and thus two prototypes were made: Normal-type with exposed electrode width of 5 mm as shown in Fig. 2 (a), and width of 0.1 mm span-type shown in Fig. 2 (b). In addition, encapsulated electrode width was set to 10 mm for both normal-type and span-type.

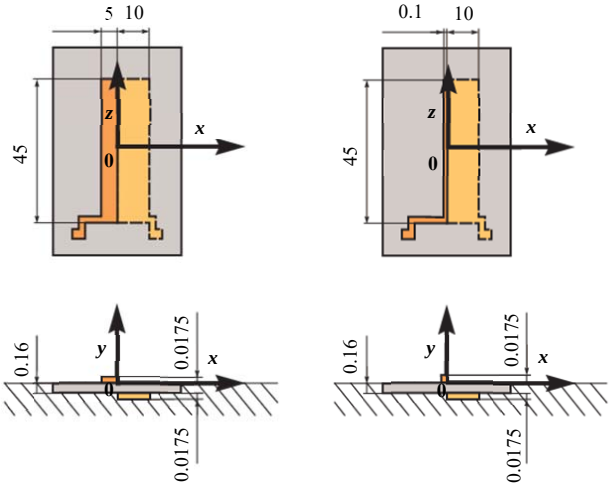

(a) Normal-type (b) Span-type

Fig. 2 DBD-PAs design

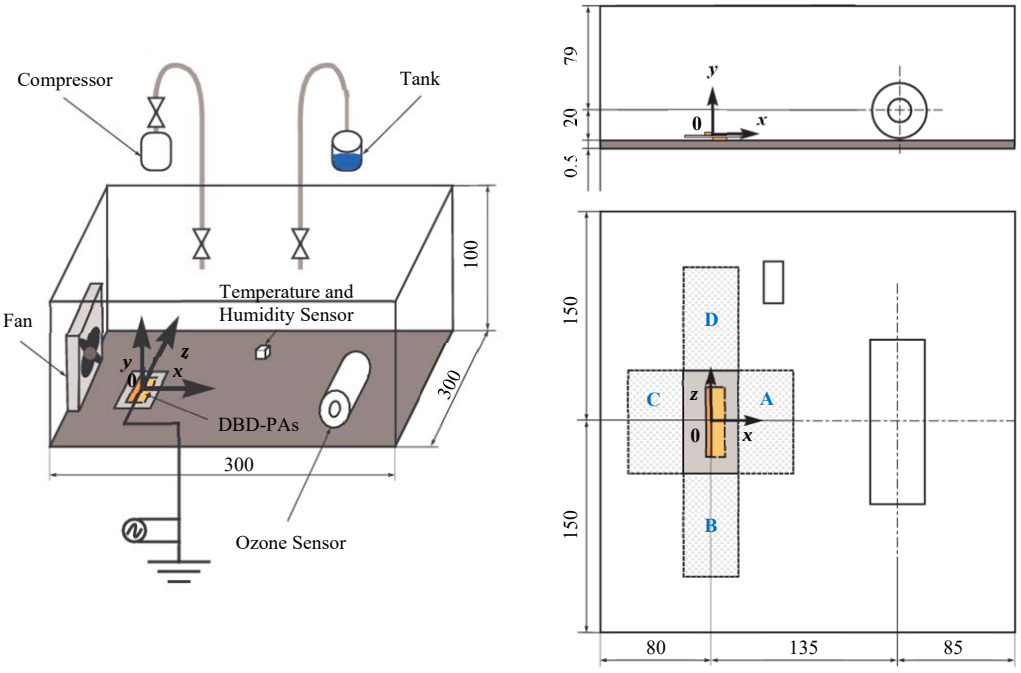

(a) A fan was provided in the container, for measuring ozone concentration with circulation of air

(b) To examine placement position, catalyst or carbon was placed as shown at a, b, c, d and ozone concentration was measured

Fig. 3 Setup for measuring ozone concentration

B. Ozone Concentration Measurement

As shown in Fig. 3, the equipment for measuring ozone concentration generated by DBD-PAs. DBD-PAs was placed so that exposed electrode edge was at position 70 mm to the left of the center of a sealed acrylic container (AS ONE Corporation, 300 × 100 × 300 mm), and the edge of the exposed electrode was taken to be the origin. The ozone concentration sensor (aeroqual, series 300, Ozone High 0-10 ppm) was placed at position x = 135 mm from exposed electrode edge of DBD-PAs, and the detection sensor part was set to face the z direction. In this experiment, concentration measurement was performed using two techniques for breaking down ozone: a case where a honeycomb catalyst (nichias corporation, ZCH2, 40 × 10 × 65 mm, 380 cell/inch^2) was provided inside the

container, and a case where a graphite sheet (AS ONE corporation, PERMA-FOIL®, 40 × 0.22 × 65 mm) was affixed. When the honeycomb catalyst was used, a stage (40 × 10 × 65 mm) designed taking into account catalyst thickness was provided to prevent any hindrance of the induced flow produced from DBD-PAs, and DBD-PAs was placed on its top side. When a graphite sheet was affixed, no stage was provided because the sheet was thin and did not interfere with the induced flow. In the experiment the air in the container was kept at temperature of T = 15 ºC, and after adjusting to humidity of RH = 30% using a compressor (HITACHI corporation, 0.2LE-8S), sine wave with peak-to-peak voltage of $V_{p\text{-}p}$ = 4.0-8.0 kV and frequency of f_p = 5.0 kHz was applied to DBD-PAs for 15 seconds, and ozone concentration was measured for the cases with a honeycomb catalyst or graphite sheet in the container, and the case when these were not used. To measure ozone concentration when ozone in the container was kept uniform, measurement was conducted in the case where air was forcibly diffused in the container using a fan with flow velocity of about 4 m/s. Taking into account the 90% response time of the sensor, measurement of ozone concentration was performed for 120 seconds at 1 second intervals.

C. PIV Measurement

The distribution of the induced flow of each DBD-PAs was analyzed using particle image velocimetry (PIV) shown in Fig. 4. DBD-PAs was placed on the stage in the acrylic container, and PIV measurement was performed in the case where a honeycomb catalyst was provided in the positive direction of the x-axis, and the case where it was not provided. In this way, the effects of the honeycomb catalyst on the induced flow were verified. Dioctyl sebacate (DOS) finely granulated to about 1 μm was introduced into the acrylic container as seeding particles for visualizing flow. A sine wave with peak-to-peak voltage of $V_{p\text{-}p}$ = 4.0-8.0 kV and frequency of f_p = 5.0 kHz was applied to DBD-PAs. The induced flow was made visible with a double-pulse Nd:YAG laser (Litron Lasers, NANO S30-15PIV, 15 mJ/pulse), and the image made visible was captured with a cross-correlation camera (TSI, PIVCAM13-8, 1280 × 1024 pixels). The velocity vector (u, v) in the x-y cross-section was found by analyzing the cross-correlation of the pairs of visualized images acquired over a short time interval.

D. Power Consumption Measurement

The power consumption of DBD-PAs was evaluated with the V-Q Lissajous method using the circuit shown in Fig. 5 [10], [11]. Capacitors for detecting charge were connected in series with DBD-PAs. Since the charge Q_{PA} charged to DBD-PAs and the charge Q_r charged to the capacitors are equal, the charge of DBD-PAs is found as $Q_{PA} = C_r V_r$ by using the known electrostatic capacity of the detection capacitors C_r. Therefore, power consumption was calculated as the product of frequency and the area surrounded by the Lissajous figure drawn by Q_{PA} and the voltage V_{PA} applied to DBD-PAs.

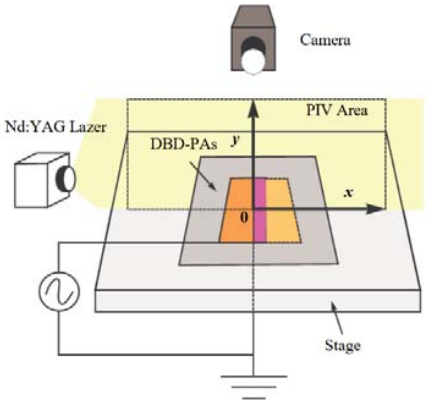

Fig. 4 PIV setup

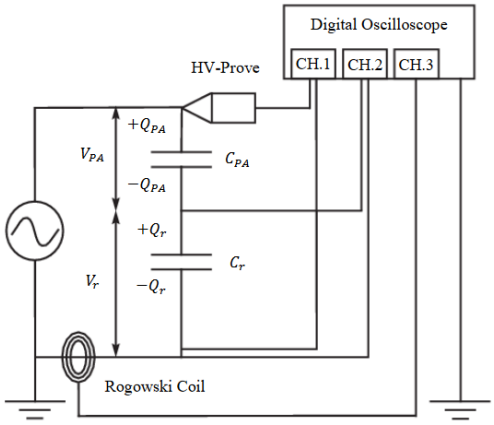

Fig. 5 Image of measuring power consumption

E. Ozone Distribution

To investigate the diffusion of ozone generated from DBD-PAs, the ozone distribution was measured by preparing ozone detection paper using indigo carmine emittance-absorption photometry [12], [13]. When the double bond in the indigo carmine molecule is broken due to chemical reaction with an active species, it becomes impossible to absorb light near 630 nm, and its hue fades from blue to transparent. This makes it possible to trace the diffusion of ozone generated from DBD-PAs by observing the whiteness of indigo carmine. Ozone detection paper was prepared by immersing 0.18 mm thick filter paper in a mixed aqueous solution (indigo carmine 0.225 g, citric acid 17.5 g, glycerine 62.5 g) and then drying using a dryer. A sine wave with Vp-p = 6.0 kV, fp = 5.0 kHz was applied to DBD-PAs for 120 seconds, and the appearance of ozone detection paper (dyed blue) fading to white due to the generated ozone was photographed with a digital camera (CANON corporation, EOS6D). In order to elucidate in three dimensions the distribution of ozone generated from DBD-PAs, exposed electrode edge of DBD-PAs was placed on the ozone detection paper (240 × 165 mm) in the x-z plane as indicated in Fig. 6, 70 mm from the left edge of the paper, and 82.5 mm from the lower edge. For the y-z plane, the distribution was elucidated by setting ozone detection paper (100 × 100 mm) at the position x = 50 mm.

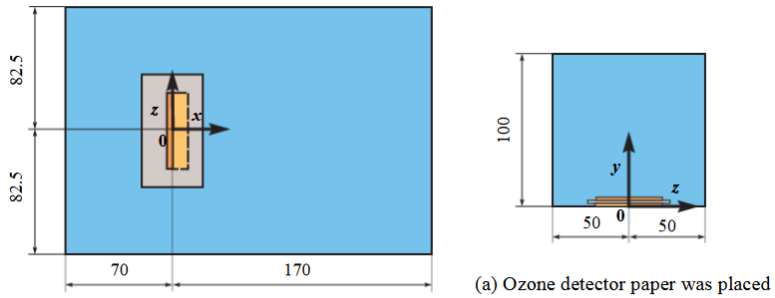

(a) Ozone detector paper was placed at x = 50 mm to reveal the ozone distribution in the y-z plane

Fig. 6 Setting position of ozone detector paper

III. Experimental Results and Discussion

A. Effects of Electrode Geometry

The relationship between maximum induced flow velocity and applied voltage for DBD-PAs in the case when a honeycomb catalyst is not provided shown in Fig. 7. As the applied voltage increases, so does the maximum induced flow velocity, and span-type is 26-84% higher than normal-type at peak-to-peak voltage of $V_{p\text{-}p}$ = 4.0-6.0 kV. Induced flow velocity is 7-10% higher with normal-type than with span-type at $V_{p\text{-}p}$ = 7.0, 8.0 kV. Hagiwara et al. have reported that when span-type was used, DBD occurs not only at the edge part in the positive direction of the x-axis (referred to below as the "downstream side") but also in the negative direction of the x-axis (referred to below as the "upstream side") [7]. Due to the occurrence of DBD on the upstream side, it was likely that induced flow also occurs not only on the upstream side but also on the downstream side, resulting in increase in induced flow velocity. The cause is not clear for why fluid does not accelerate due to increased voltage, but it is evident that, at least at $V_{p\text{-}p}$ = 4.0-6.0 kV, refining the exposed electrode structure results in higher induced flow velocity.

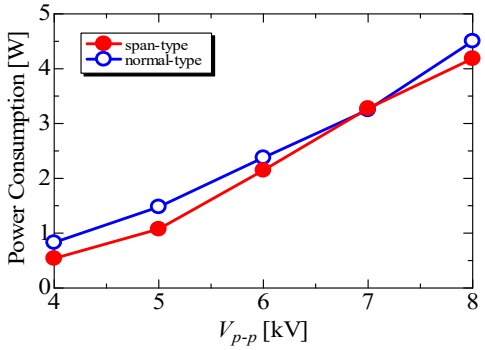

Fig. 7 Relation between maximum velocity and voltage

Fig. 8 shows the relationship between DBD-PAs power consumption and applied voltage. It was evident that power consumption increases as applied voltage increases, but span-type was driven with less power consumption than normal-type. The reduction in power consumption of span-type is thought to be attributable to electrostatic capacity. Electrostatic capacity when DBD-PAs was driven with appliedpeak-to-peak voltage of $V_{p\text{-}p}$ = 4.0 kV and frequency of f_p = 5.0 kHz was calculated from the slope of the approximation line of the Lissajous figure, and the results showed that while electrostatic capacity of normal-type was 28.5 pF, that for span-type was 19.1 pF. It was likely that span-type was driven with lower power consumption due to the reduction in electrostatic capacity.

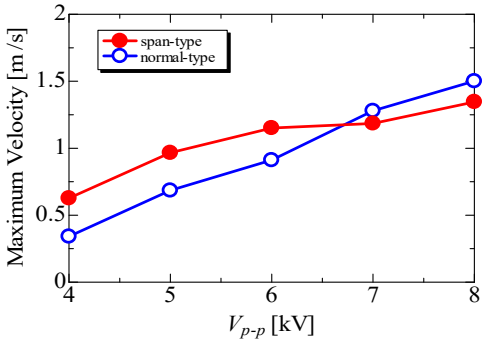

Fig. 8 Relation between power consumption and voltage

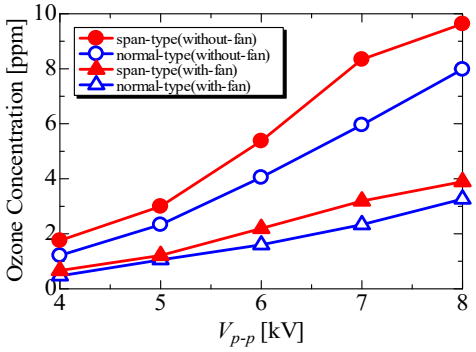

Fig. 9 Relation between ozone concentration and voltage

The relationship between the maximum ozone concentration measured with the ozone concentration sensor and applied voltage is shown in Fig. 9. The higher the applied voltage, the more ozone concentration increases. This finding indicates as applied voltage increases, there was greater dissociation of

oxygen molecules in the air due to electrons during discharge. If a fan was used inside the container, the ozone concentration was lower than the case where it was not used, and broader diffusion of ozone can be confirmed in the container due to a fan. If a fan was not used, the difference in concentration between span-type and normal-type was large 0.5-3.3 ppm, and if a fan was used, the difference in concentration was small 0.2-0.9 ppm. This is thought to be because ozone concentration per unit spatial volume decreases due to diffusion of ozone in the container. Span-type had a higher ozone concentration of 18-45% compared to normal-type. This was likely because span-type had a larger plasma generation region than normal-type [7].

To clarify the relationship between induced flow velocity and amount of ozone generated, the situation was examined in terms of the ratio of induced flow velocity and ozone concentration. Fig. 10 shows the relationship with DBD-PAs power consumption. It was evident that the ratio of induced flow velocity and ozone concentration was not fixed, and tends to increase with higher applied voltage and power consumption. Compared to normal-type, span-type had small 9-21% ratio of induced flow velocity and ozone concentration at V_{p-p} = 4.0, 5.0 kV. However, span-type had larger ratio of induced flow velocity and ozone concentration (5-51%) than normal-type at V_{p-p} = 6.0-8.0 kV. For this reason, it was evident that, at a low applied voltage of V_{p-p} = 4.0, 5.0 kV, span-type had a lower ozone concentration relative to the maximum induced flow velocity and lower power, whereas at high voltage such as V_{p-p} = 6.0-8.0 kV, normal-type had smaller ozone concentration relative to the maximum induced flow velocity.

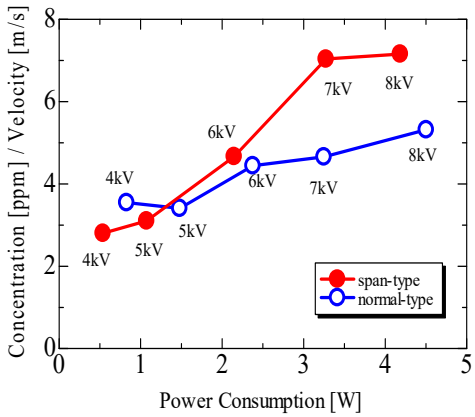

Fig. 10 Relation between concentration rate per velocity and power consumption

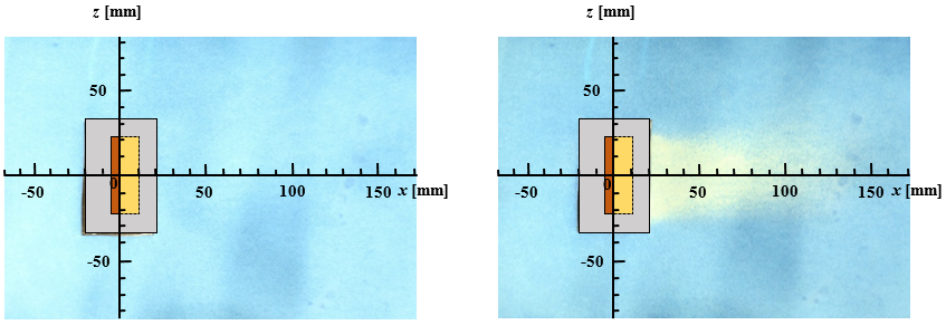

(a) 0 sec (b) 120 sec

Fig. 11 Distribution of ozone in the *x*-*z* plane (normal-type)

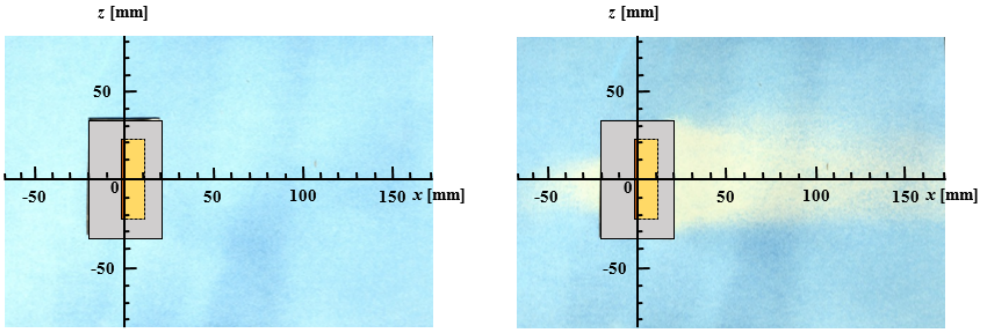

(a) 0 sec (b) 120 sec

Fig. 12 Distribution of ozone in the *x*-*z* plane (span-type)

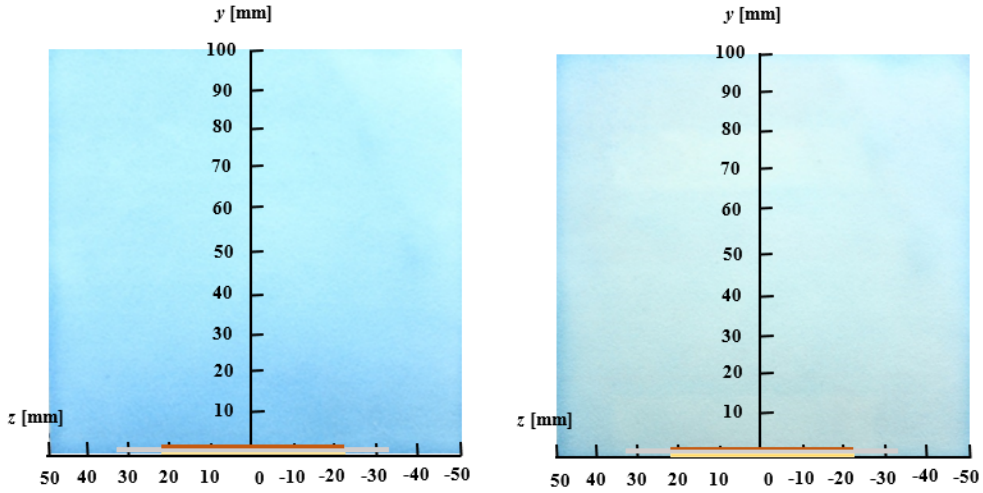

(a) 0 sec (b) 120 sec

Fig. 13 Distribution of ozone in the *y-z* plane (normal-type, $x = 50$ mm)

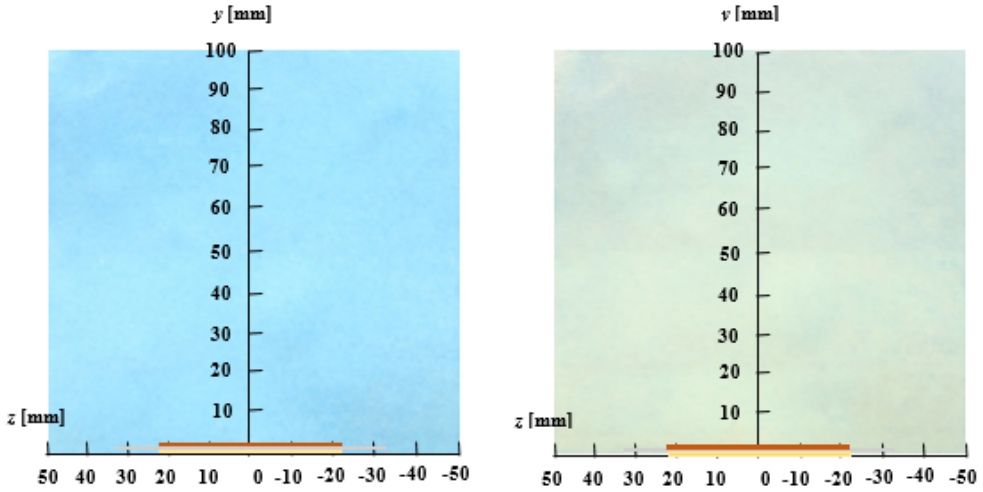

(a) 0 sec (b) 120 sec

Fig. 14 Distribution of ozone in the *y-z* dimension (span-type, $x = 50$ mm)

B. Ozone Distribution

With regard to the ozone distribution (*x-z* plane), Fig. 11 shows the change in color of the ozone detection paper for normal-type, and Fig. 12 shows the same for span-type. Figs. 11 (a) and 12 (a) show the change in ozone detection paper color before driving DBD-PAs, and Figs. 11 (b) and 12 (b) show the same change 120 seconds after drive. It was evident from Fig. 11 and 12 that there was a marked fading to white of the ozone detection paper near DBD-PAs. It can be confirmed that there was fading to white up to about $x = 80$ mm with normal-type from Fig. 11, while with span-type shown in Fig. 12, there was fading to white up to about $x = 110$ mm, and even fading on the upstream side. Compared to normal-type, span-type has a high maximum induced flow velocity and ozone concentration, as is evident from Figs. 6 and 8, and thus it is conjectured that the distribution covers a wide range. Due to the fact that Hagiwara et al. have shown that induced flow was generated on the upstream side by using fine exposed electrode, it was likely that ozone was also distributed on the upstream side with span-type [7].

Fig. 13 shows the change in color of ozone detection paper in the *y-z* plane at $x = 50$ mm for normal-type, and Fig. 14 shows the same for span-type. It can be confirmed that the ozone detection paper fades to white uniformly for both normal-type and span-type from Figs. 13 and 14. Compared to normal-type, span-type has more marked whitening of the ozone detection paper, and thus it is suggested that the distribution has high ozone concentration in the *y* direction as well.

C. Ozone Concentration Reduction using Honeycomb Catalyst and Carbon Sheet

The appropriateness of the setup positions of the honeycomb catalyst and carbon sheet for breaking down ozone was

examined, as shown in Fig. 3, by varying the position between DBD-PAs' downstream side (point A), right side (point B), upstream side (point C) and left side (point D). The experiment conditions were peak-to-peak voltage of $V_{p\text{-}p}$ = 8.0 kV and frequency of f_p = 5.0 kHz. This was because, with reduction of ozone concentration using honeycomb catalyst, ozone generated from DBD-PAs was changed to oxygen due to honeycomb catalyst (M) reaction in (1):

$$2O_3 + M \rightarrow M + 3O_2 \quad (1)$$

This was also because, with reduction in ozone concentration using carbon sheet, ozone changes to carbon dioxide and oxygen due to a carbon reaction, as shown in (2):

$$C + 2O_3 \rightarrow CO_2 + 2O_2 \quad (2)$$

There was a major drop in the reduction rate at other positions, compared to the case when set up on the downstream side (point A) from Figs. 15 and 16. This shows that placing a honeycomb catalyst or carbon sheet on the downstream side has a large effect in reducing ozone concentration.

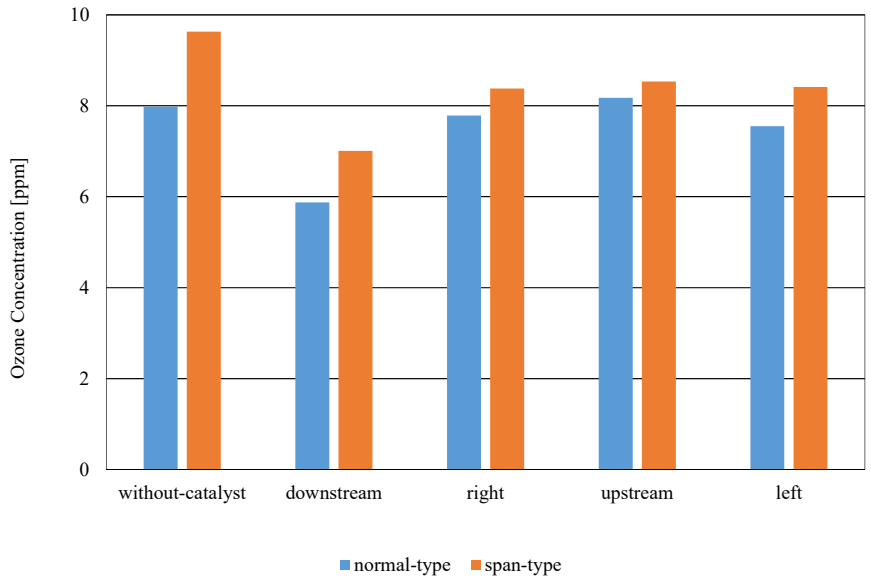

Fig. 15 Effect of honeycomb catalyst on ozone concentration

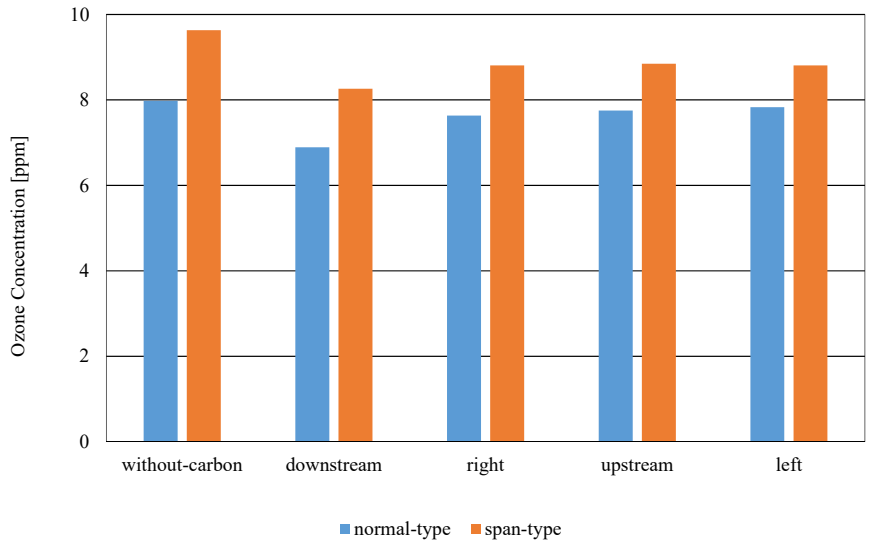

Fig. 16 Effect of carbon sheet on ozone concentration

If honeycomb catalyst or carbon sheet was placed on the downstream side in the container there is a large effect in reducing ozone concentration. Therefore, honeycomb catalyst or carbon sheet was placed on the downstream side, and changes in ozone concentration were measured for 1 hour. Experiment conditions were: normal-type, $V_{p\text{-}p}$ = 8.0 kV, f_p = 5.0 kHz. Fig. 17 shows changes over time in ozone concentration in the cases where honeycomb catalyst or carbon sheet was provided, and the case when nothing was provided. It was evident that, in all conditions, about 80 seconds was necessary from the start of DBD-PAs drive until ozone concentration reaches its maximum, if the 90% response time of the sensor was taken into account. It takes ozone concentration in the container about 1 hour to return to the pre-experiment concentration from Fig. 17. If a honeycomb catalyst was used which yields a high percentage reduction of ozone concentration, then it can be confirmed that time to reduction was short, and the reduction effect was large.

Relationship between ozone concentration in the presence or absence of set of honeycomb catalyst or carbon sheet in downstream side of DBD-PAs in container and applied voltage shown in Fig. 18. Fig. 18 (a) normal-type, Fig. 18 (b) span-type was ozone concentration with honeycomb catalyst, normal-type 18-42%, span-type 22-31% of ozone concentration was reduced. On the other hand, placing carbon sheet reduced ozone concentration normal-type of 4-14%, span-type of 8-14% reduces ozone concentration, as compared to carbon plate, towards catalyst was large reduction effect. In addition, reduced ozone concentration to increase with increase of applied voltage.

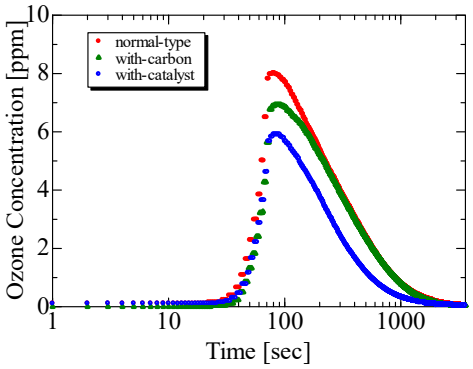

Fig. 17 Time variation of ozone concentration (normal-type, $V_{p\text{-}p}$ = 8.0 kV, f_p = 5.0 kHz)

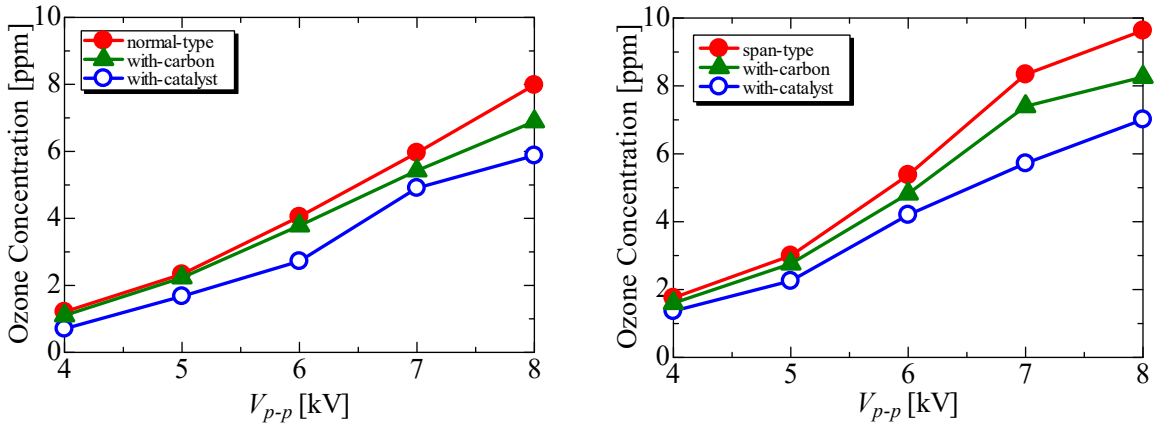

(a) normal-type (b) span-type

Fig. 18 Effect of catalyst or carbon on ozone concentration

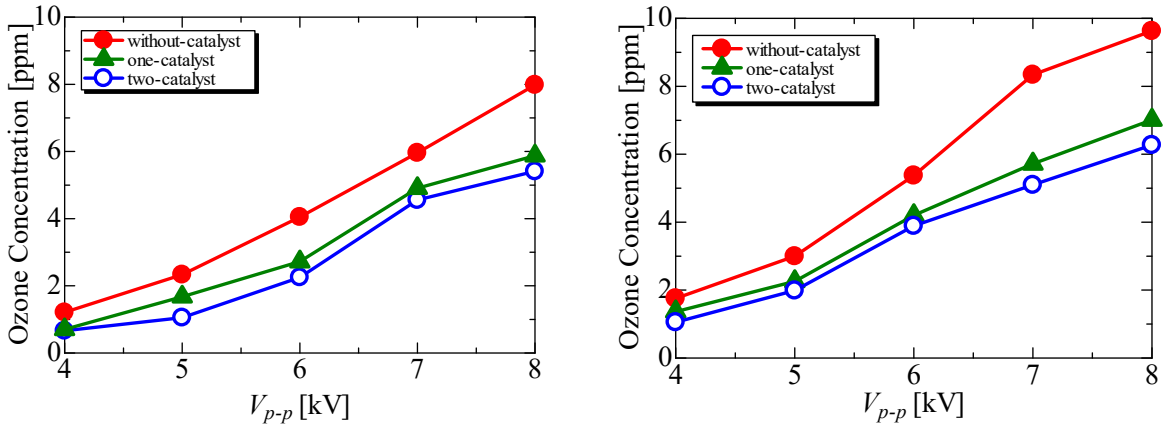

(a) normal-type (b) span-type

Fig. 19 Effect on number of catalyst on ozone concentration

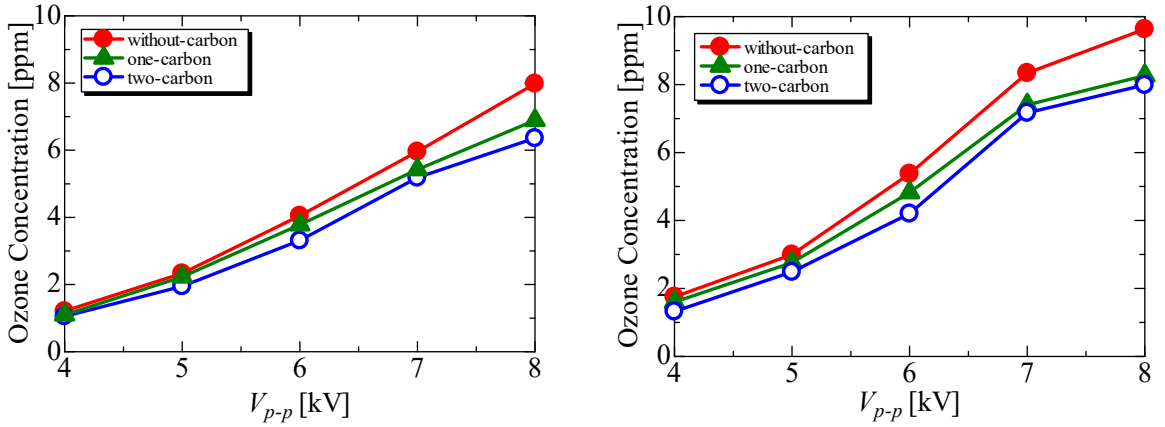

(a) normal-type (b) span-type

Fig. 20 Effect on number of carbon on ozone concentration

Figs. 10 and 11 show that ozone was diffused up to about x = 80-110 mm, and for this reason the effect of reducing ozone concentration was verified by changing the number of honeycomb catalysts or carbon sheets placed on the downstream side. Figs. 19 (a) and 20 (a) show the relationship between ozone concentration and applied voltage when normal-type is used, and 0-2 honeycomb catalysts or carbon sheets are placed on the downstream side. Figs. 19 (b) and 20 (b) show the relationship between ozone concentration and applied voltage when span-type is used and varying number of honeycomb catalysts or carbon sheets are provided. Figs. 19 (a) and (b) show that when 2 honeycomb catalysts were provided, ozone concentration was reduced by 24-55% with normal-type, and by 28-40% with span type. On the other hand, Figs. 20 (a) and (b) show that, when 2 carbon sheets were provided, ozone concentration was reduced in the range 13-22% with normal-type, and 14-24% with span-type. From this it can be confirmed that the reduction in ozone concentration was greater when 2 items (catalyst or carbon sheet) were provided on the downstream side than when 1 item was provided. Thus, it was likely that honeycomb catalyst or carbon sheet contact area had an effect on reduction in ozone concentration.

To clarify the effects of ozone concentration on induced flow velocity, PIV measurement was used to analyze the spatial velocity distribution when the honeycomb catalyst was and was not present (Fig. 21). Experiment conditions were: normal-type, $V_{p\text{-}p}$ = 8.0 kV, f_p = 5.0kHz. The exposed electrode edge where DBD was generated was placed at x = 15 mm. Between the two conditions, the condition (Fig. 21 (a)) where no honeycomb catalyst was placed on the downstream side and the condition (Fig. 21 (b)) where a honeycomb catalysts was provided, no difference was evident in the velocity distribution, and thus it was confirmed that honeycomb catalyst had almost no effect on induced flow. This indicated the possibility of reducing ozone concentration without reducing the induced flow velocity of DBD-PAs.

IV. Conclusion

In this study, DBD-PAs with two types of exposed electrode structure measured ozone concentration, power consumption and maximum induced flow velocity, and effectiveness in reducing ozone concentration was verified by placing honeycomb catalyst and carbon sheet on the downstream side. Ozone distribution was also examined by preparing ozone detection paper, and observing changes in the paper's color. Ozone was distributed on the downstream side with both normal-type and span-type, and the concentration was high near DBD-PAs, but it was confirmed that ozone diffuses even on the upstream side of span-type. Span-type had lower power consumption, higher ozone concentration, and higher induced flow velocity than normal-type at $V_{p\text{-}p}$ = 4.0-6.0 kV. On the other hand, normal-type had higher induced flow velocity and lower ozone concentration than span-type at $V_{p\text{-}p}$ = 7.0, 8.0 kV. It was confirmed that placing a honeycomb catalyst or carbon sheet near the electrode in the downstream direction reduces ozone concentration by 18-42% without affecting induced flow.

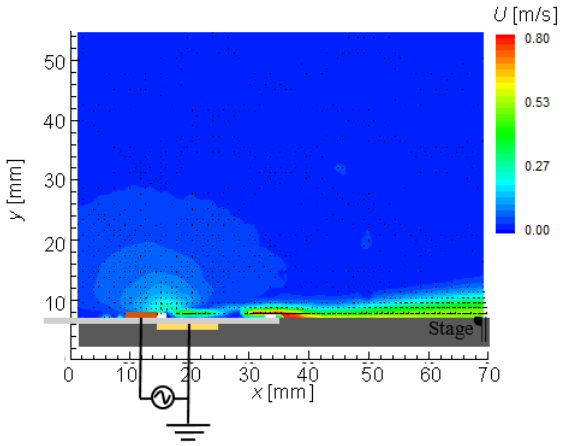

(a) without-catalyst

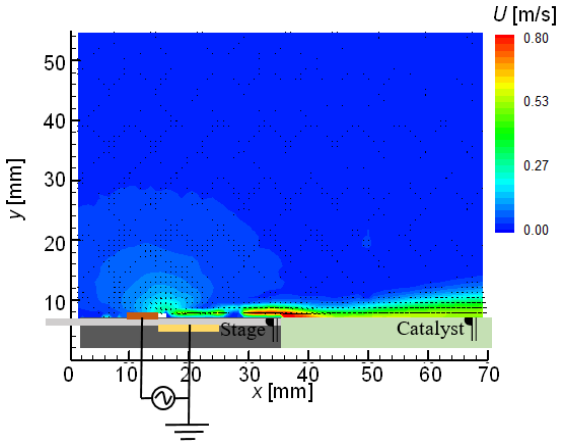

(b) with-catalyst

Fig. 21 Velocity profile (normal-type, $V_{p\text{-}p}$ = 6.0 kV, f_p = 5.0 kHz)

Acknowledgment

This research was supported by a grant for advanced industrial technology development from the New Energy and Industrial Technology Development Organization (NEDO) of Japan. The specific grant was for "Research and development to achieve rapid startability and improved equipment utilization for wind power generation systems through virtual blade construction using active fluid control technology (11B04022c)."

References

[1] Roth, J. R. and Dai, X., "Optimization of the aerodynamic plasma actuator as an electrohydrodynamic (EHD) electrical device," *44th AIAA Aerospace Sciences Meeting and Exhibit*, pp. 9 - 12, 2006.
[2] Gad-El-Hak, M., "Flow Control," *Cambridge University Press*, 2000.
[3] Glezer, A. and Amitay, M., "synthetic jets," *Annu. Rev. Fluid Mech*, vol. 34, pp. 503 - 529, 2002.
[4] Suzuki, H., Kasagi, N. and Suzuki, Y., "Active control of an axisymmetric jet with distributed electromagnetic flap actuators," *Exp. Fluids*, vol. 36, pp. 498 - 509, 2004.
[5] Kasagi, N., Suzuki, Y. and Fukagata, K., "Microelectromechanical systems-based feedback control of turbulence for skin friction reduction," *Annu. Rev. Fluid Mech*, vol. 41, pp. 231 - 251, 2009.
[6] Fukagata, K., Yamada, S. and Ishikawa, H., "Plasma Actuators: Fundamentals and Research Trends," *nagare*, vol. 29, no. 4, pp. 243 - 250, 2010.
[7] Hagiwara, H., Ogata, S. and Segawa, T., "Properties of Flows Induced by DBD Plasma Actuators with Fine Structural Exposed Electrodes," *45th AIAA Plasmadynamics and Lasers Conference*, AIAA2014 - 2667, 2014.
[8] Kawamoto, H. and Kobayashi, T., "Ozone Generation in Plasma Actuator", *Transactions of the JSME B*, vol.75, no. 759, pp. 2345 - 2347, 2009.
[9] Nicole, M. H., Philippe, L., Rogerio, P., Yves, D. V. and Tommy, R., "Electromagnetic and Ozone Emissions from Dielectric Barrier Discharge Plasma Actuators (RTO)," *45th AIAA Plasmadynamics and Lasers Conference*, AIAA2014 - 2809, 2014.
[10] Kriegseisa, J., Möllera, B., Grundmannb, S. and Tropea, C., "Capacitance and Power Consumption Quantification of Dielectric Barrier Discharge (DBD) Plasma Actuators," *Journal of Electrostatics*, vol. 69, no. 4, pp. 302 - 312, 2011.
[11] Ashpis, D. E., Laun, M. C. and Griebeler, E. L., "Progress toward Accurate Measurements of Power Consumptions of DBD Plasma Actuators," *50th AIAA Aerospace Sciences Meeting*, AIAA2012 - 0823, 2012.
[12] Mizuniwa, F., Sakai, K., Umino, T. and Sugawara, Y., "Spectrophotometric determination of dissolved oxygen in water with indigo carmine," *Analytical Chemistry*, vol. 2, no. 2, pp. 89 - 93, 1976.
[13] Maruo, Y., Kunioka, T., Akaoka, K. and Nakamura, J., "Development and evaluation of ozone detection paper," *Sensors and Actuators B*, vol. 135, pp. 575 - 580, 2009.